



Data-driven imaging with second-order traveltimes approximations – traveltimes derivatives and kinematic wavefield attributes

Jürgen Mann* and Yonghai Zhang, Geophysical Institute, University of Karlsruhe

Copyright 2003, SBGf – Sociedade Brasileira de Geofísica

This paper was prepared for presentation at the 8th International Congress of The Brazilian Geophysical Society held in Rio de Janeiro, Brazil, September 14-18 2003.

Contents of this paper was reviewed by The Technical Committee of the 8th International Congress of The Brazilian Geophysical Society and does not necessarily represent any position of the SBGf, its officers or members. Electronic reproduction, or storage of any part of this paper for commercial purposes without the written consent of The Brazilian Geophysical Society is prohibited.

Summary

Starting with the general concept of second-order traveltimes approximations for seismic reflection imaging, we discuss the number of determinable parameters, i. e., spatial derivatives of the traveltimes, for different acquisition geometries, e. g., narrow azimuth 3-D marine data or full azimuth 3-D data, and processing approaches ranging from the most general multi-parameter problem down to the well-known single-parameter approach used in the common-midpoint stack. With the help of the near-surface velocity (or both, P and S wave velocities in case of converted waves), these derivatives can be related to spatial properties of various kinds of hypothetical wavefronts observed at the acquisition surface. This constitutes the basis for a number of recently introduced data-driven imaging methods that differ in the derivation and representation of their traveltimes approximations, but not in their general principles. Our aim is to present the current state of the art of one of the available implementations, the Common-Reflection-Surface Stack, followed by two application examples that demonstrate the advantages of the formulation in terms of wavefront properties.

Introduction

Seismic reflection imaging methods based on traveltimes approximations of second order have been commonly used for decades: the classic common-midpoint (CMP) stack or the normal moveout(NMO)/dip moveout(DMO)/stack sequence can be seen as such processes, although their data-driven aspects are often not fully exploited. In recent years, several methods emerged that overcome many of the limitations of the classic approaches and go beyond the restriction to certain subsets of the pre-stack data. Instead of only one parameter, the stacking velocity, an entire set of kinematic wavefield attributes allows to locally approximate the reflection response of the subsurface for arbitrary source and receiver configurations. These attributes, associated with first and second spatial derivatives of the traveltimes, can be directly determined from the pre-stack data such that no explicit parameterization of the depth model is required. The physical interpretation of the attributes in terms of propagation directions and wavefront curvatures provides information that serves for various applications like inversion, migration etc. Thus, stacking of the pre-stack data is only one aspect in data-driven imaging based on second-order traveltimes approximations.

Basic concepts

A second-order traveltimes approximation with respect to an arbitrarily chosen point P on a reflection event in the pre-stack data can be described by any (hyper-)surface that includes the point P itself and coincides with the actual reflection event with respect to its first and second spatial derivatives at P . The surface fitting best the actual reflection events, together with the spatial derivatives that serve as its parameters, can be determined by means of a coherence analysis within an appropriate aperture in the pre-stack data.

In the most general case of 3-D acquisition with full azimuth coverage, the pre-stack data consists of a 5-D hyper-volume spanned by the traveltimes t , the source coordinates \vec{s} , and the receiver coordinates \vec{g} , both given by vectors with two components, considered to be located on a plane measurement surface for the moment. Thus, four first spatial derivatives and nine second spatial derivatives are required to fully describe a second-order approximation of the traveltimes. For the corresponding 2.5-D problem, this reduces to two first and three second spatial derivatives. If we express the coordinates in terms of midpoint $\vec{\xi} = (\vec{g} + \vec{s})/2$ and half-offset $\vec{h} = (\vec{g} - \vec{s})/2$, further simplifications occur if we address the particular problem of zero-offset (ZO) simulation, where shot and receiver coordinates of P coincide: due to the reciprocity of traveltimes, the first derivatives with respect to \vec{h} and the mixed second derivatives including \vec{h} vanish. Accordingly, two first derivatives and six second derivatives remain in 3-D, and one first and two second derivatives in 2.5-D. Restricting our traveltimes approximation in the latter case to the CMP gathers only, we end up with a single second derivative which is traditionally interpreted in terms of stacking velocity—simply a special case of the general second-order approach. If only subsets of the full 5-D data hyper-volume are acquired and/or processed, for example in case of 3-D marine acquisition along parallel lines, the number of determinable derivatives obviously also reduces. Table 1 summarizes the number of dimensions of the pre-stack data volume and the number of determinable derivatives for different acquisition geometries. The numbers in parentheses refer to the special case of ZO simulation.

The representation of the stacking surface can be chosen in several ways. Depending on the derivation of the traveltimes approximation, either geometrical or by means of the ray propagator formalism of paraxial ray theory, one obtains double-square-root expressions like in Multifocusing (Berkovitch et al., 1994; Landa et al., 1999) or different kinds of quadrics of parabolic and hyperbolic form (Schleicher et al., 1993; Höcht et al., 1999). Although some of these expressions are exact for very simple situations, it is not evident which of these alternatives generally leads to the best possible results.

Acquisition geometry	Data space	Number of derivatives
3-D, full azimuth coverage	5-D	13 (8)
3-D, narrow azimuth coverage	4-D	7 (6)
2-D line	3-D	5 (3)

Table 1: Number of dimensions of the pre-stack data volume and the number of determinable derivatives for different acquisition geometries. The numbers in parentheses refer to the special case of ZO simulation. In case of narrow azimuth acquisition geometry, an additional first spatial derivative with respect to the crossline offset might be considered.

Physical interpretation of the derivatives

So far, the entire imaging problem has been described in terms of traveltimes derivatives without any physical interpretation. However, such an interpretation is mandatory if we want to be able to decide which values of the derivatives are reasonable for (primary) reflection events and, thus, worthwhile to be considered during the search for the optimum parameters. Furthermore, this approach provides information about the properties of the reflectors and their overburden and allows additional generalizations that account, e. g., for the topography of the acquisition surface.

Introducing a near-surface velocity v_0 , assumed to be known and almost constant inside the aperture, we can readily relate the first spatial derivatives (often also called horizontal slownesses) to the incidence and emergence directions of wavefronts originating from hypothetical experiments, measured at the known source and receiver positions associated with P . Accordingly, the second derivatives can be related to the curvatures of these wavefronts. In other words, v_0 is the link between the spatial traveltimes derivatives and spatial properties of wavefronts at the acquisition surface. The latter are also called *kinematic wavefield attributes*. In the hypothetical experiments, wave propagation is considered along a central ray connecting the source and receiver associated with P . Nevertheless, the properties of the actual central ray are not required and no ray tracing is involved.

There are various real and hypothetical experiments that can be associated with the spatial derivatives of traveltimes. For the sake of simplicity, we restrict ourselves to the maybe simplest interpretation that can be used for the case of ZO simulation: here, the second derivatives with respect to \bar{h} can be related to a wavefront emanating from a point source at the (unknown) reflection point in depth (the so-called NIP wave experiment), whereas the derivatives with respect to $\bar{\xi}$ locally describe a wavefront originating from an exploding reflector (the so-called normal wave experiment). The first derivatives with respect to $\bar{\xi}$ enter into the description of both wavefronts. Details on these experiments can, e. g., be found in Hubral (1983). Obviously, the concept of such experiments is well suited for inversion algorithms, either by downward propagation of the wavefronts until they satisfy an imaging condition (for the above example, the focusing of the NIP wavefront at time zero) in a generalized Dix-type inversion (Biloti et al., 2002), or by tomographic approaches that are based on the forward-modeling of the wavefronts (Duveneck and Hubral, 2002) by means of dynamic ray tracing.

Implementation strategies

The determination of the traveltimes derivatives (or, alternatively, of the wavefield attributes) from the pre-stack data is

a multi-parameter non-linear global optimization problem. The crucial task is to solve this optimization problem in a reasonable amount of time while preserving a sufficient accuracy of the results. There is no unique way to address this task for all kinds of acquisition geometries. Nevertheless, the use of subsets of the pre-stack data with sufficient coverage in each subset to determine the wavefield attributes step by step appears to be an appropriate strategy in many cases. For instance, the existing ZO implementations of the CRS stack in 2-D and 3-D determine the wavefield attributes step by step starting with CMP gathers/volumes followed by an analysis of the resulting ZO section/volume (see, e. g., Jäger et al., 2001; Cristini et al., 2001). In conflicting dip situations, an additional search in common-shot/common-receiver gathers/volumes helps to determine local coherence maxima (Mann, 2001). For the more general problem of non-zero offsets, similar strategies are applied in the common-shot, common-offset, and CMP gathers (Zhang et al., 2001). The non-zero offset approach also allows to handle converted waves (Bergler et al., 2002). For certain acquisition geometries, the attribute search for the 3-D case can be partly or entirely decomposed into 2-D configurations, again significantly simplifying the optimization problem to be solved.

The relevant traveltimes expressions are available for the most general case, in other words, arbitrary offset, i. e., an arbitrarily chosen central ray, and 3-D acquisition with full azimuth coverage. The topography of the acquisition surface can be consistently considered from the very beginning. Concerning implementation and application, the CRS stack is currently available for 2-D ZO simulation (including topography and redatuming to a plane datum), 2-D finite-offset simulation, and 3-D ZO simulation.

Application examples

As already mentioned above, the physical interpretation of the derivatives in terms of wavefield attributes can be used for various applications, either during the stacking (e. g., to estimate the projected Fresnel zone as optimum stacking aperture) or in subsequent processes like inversion. In the scope of this abstract, we focus on the explicit consideration of topography in the 2-D ZO CRS stack. To demonstrate this technique, we used a synthetic 2-D model with four homogeneous layers. The model depicted in Figure 1 shows that the subsurface structures are not very complex. However, the topography of the acquisition surface has significant small-scale variations. As can be clearly seen from Figure 2, the reflection events are, due to the topography, far from being hyperbolic. A direct application of a second-order stacking operator within a reasonable aperture will most likely fail—static corrections and/or redatuming would have to be applied before.

With the help of the wavefield attributes, the second-order

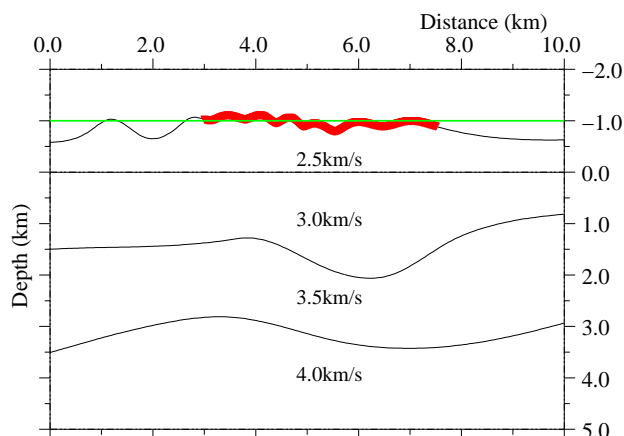


Figure 1: Model used for the synthetic data example. The red part of the acquisition line was used for the examples in Figures 3a and b, the green line depicts the redatuming level used for the results shown in Figure 3b.

traveltime approximation can be generalized to contain traveltime corrections that depend on the source and receiver elevations (Zhang et al., 2002). The number of wavefield attributes remains the same, no additional search is required. Although the CRS operator (red surface in Figure 2) is still based on a second-order approximation, it takes a rather complicated form and adapts well to the reflection event. As a consequence, the stacked section (Figure 3a) represents a ZO simulation of high quality, still attached to the actual topography.

The wavefront attributes and the associated traveltime derivatives are obtained as if the data were recorded on a plane surface with floating datum. Thus, most of the complexity introduced by the topography is already removed in the attributes. This allows to apply a redatuming to a plane datum, almost without additional effort: the redatumed section in Figure 3b is indeed a good approximation of the ZO section forward-calculated *without* topography.

Conclusions

We reviewed the basic concepts of second-order traveltime approximations and their application in data-driven seismic reflection imaging. With the assumption of a known and (locally) constant near-surface velocity, a link between the spatial first and second derivatives of the analytic traveltime approximation and the spatial properties of hypothetical wavefronts, called kinematic wavefield attributes, can be established that allow a variety of applications. We showed two examples of the use of these concepts: the generalization of the second-order traveltime approximation of the CRS stack to situations with topography and the redatuming of the stack result to a plane datum. These generalizations are not possible without (implicitly or explicitly) moving from spatial derivatives of the traveltime to spatial wavefront properties and, thus, clearly demonstrate the advantage of this concept.

Acknowledgments

We would like to thank the sponsors of the Wave Inversion Technology (WIT) Consortium for their support.

References

- Bergler, S., Duveneck, E., Höcht, G., Zhang, Y., and Hubral, P. (2002). Common-Reflection-Surface stack for converted waves. *Stud. geophys. geod.*, 46:165–175.
- Berkovitch, A., Gelchinsky, B., and Keydar, S. (1994). Basic formulae for multifocusing stack. In *Extended Abstracts*. 56th Mtg. Eur. Assoc. Expl. Geophys. Session: P140.
- Biloti, R., Santos, L. T., and Tygel, M. (2002). Multiparametric traveltime inversion. *Stud. geophys. geod.*, 46:177–192.
- Cristini, A., Cardone, G., Chira, P., Hubral, P., and Marchetti, P. (2001). 3D zero-offset Common Reflection Surface Stack for land data. In *Workshop on velocity model independent imaging for complex media*, *Extended Abstracts*, Session W5-13, <http://www.seg.org/research/2001/W5>. Soc. of Expl. Geophys.
- Duveneck, E. and Hubral, P. (2002). Tomographic velocity model inversion using kinematic wavefield attributes. In *72nd Ann. Internat. Mtg., Soc. Expl. Geophys., Expanded Abstracts*, pages 862–865.
- Höcht, G., de Bazelaire, E., Majer, P., and Hubral, P. (1999). Seismics and optics: hyperbolae and curvatures. *J. Appl. Geoph.*, 42(3,4):261–281.
- Hubral, P. (1983). Computing true amplitude reflections in a laterally inhomogeneous earth. *Geophysics*, 48(8):1051–1062.
- Jäger, R., Mann, J., Höcht, G., and Hubral, P. (2001). Common-reflection-surface stack: Image and attributes. *Geophysics*, 66(1):97–109.
- Landa, E., Gurevich, B., Keydar, S., and Trachtman, P. (1999). Application of multifocusing method for subsurface imaging. *J. Appl. Geoph.*, 42(3,4):283–300.
- Mann, J. (2001). Common-Reflection-Surface Stack and conflicting dips. In *Extended Abstracts*, Session P 077. 63rd Mtg. Eur. Assn. Geosci. Eng.
- Schleicher, J., Tygel, M., and Hubral, P. (1993). Parabolic and hyperbolic paraxial two-point traveltimes in 3D media. *Geophys. Prosp.*, 41(4):495–514.
- Zhang, Y., Bergler, S., and Hubral, P. (2001). Common-Reflection-Surface (CRS) stack for common-offset. *Geophys. Prosp.*, 49(6):709–718.
- Zhang, Y., Höcht, G., and Hubral, P. (2002). 2D and 3D ZO CRS stack for a complex top-surface topography. In *Extended Abstracts*, 64th Mtg. Eur. Assn. Geosci. Eng., Session P166.

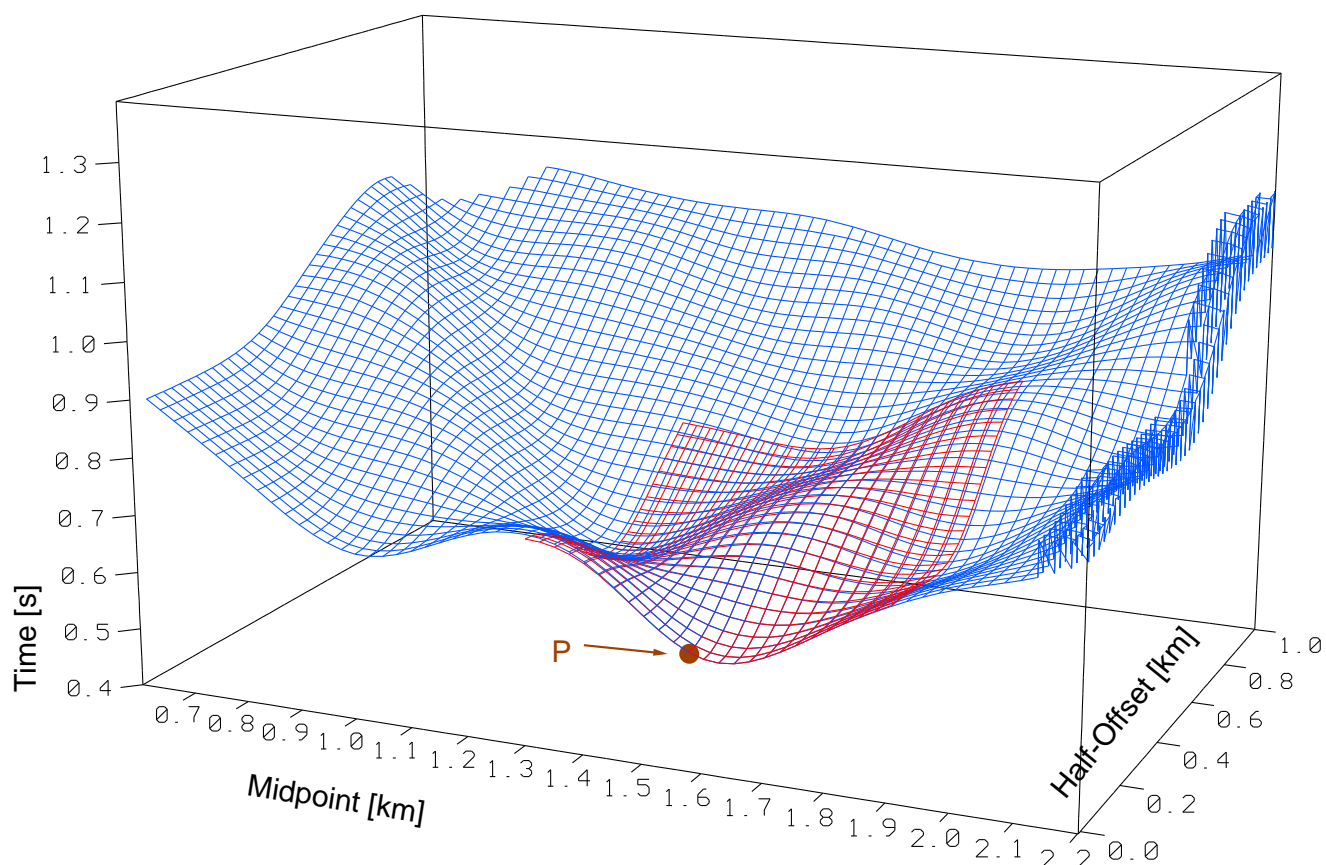


Figure 2: Reflection event (blue surface, corresponding to the uppermost reflector of the model depicted in Figure 1) in the (t, ξ, h) -domain with non-hyperbolic moveout due to topography. The wavefield attributes allow to consider the topography such that the complex event can still be approximated with a generalized second-order traveltimes approximation (red).

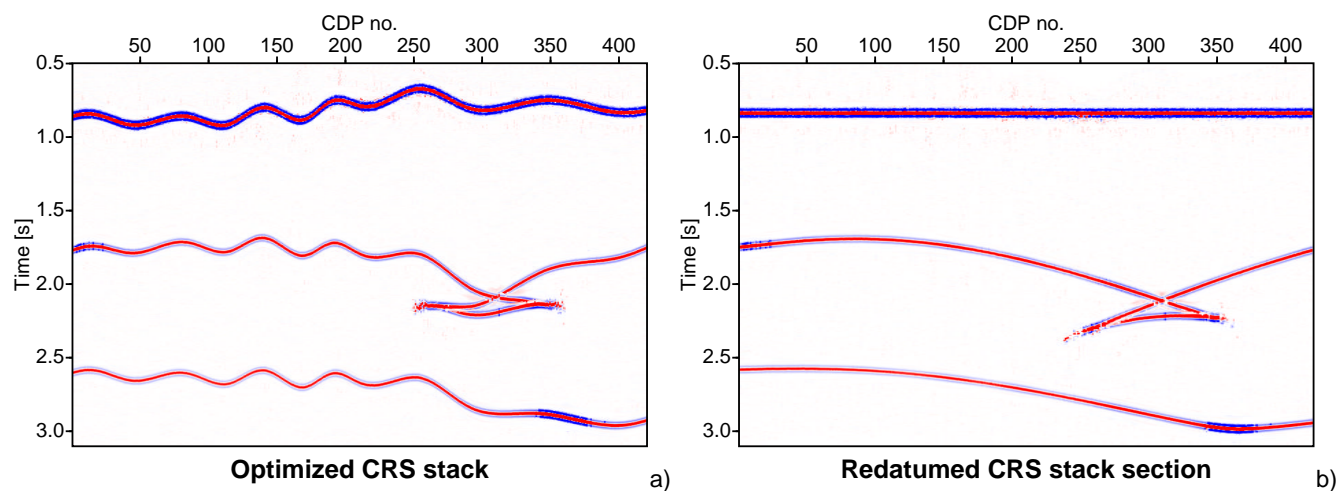


Figure 3: ZO section simulated for the four layer model shown in Figure 1: a) without and b) with redatuming based on the wavefield attributes. The chosen datum level is shown as green line in Figure 1. The redatumed section is equivalent to the same data forward-calculated to the datum level instead of the actual topography.